Title:

Mechanochemical synthesis of a mercury(II) metal-organic framework reveals a two-dimensional polymorph stabilized by weak interactions

Authors:

Isaiah R. Speight, ^a Igor Huskić, ^b Mihails Arhangelskis, ^b Hatem M. Titi, ^b Robin S. Stein, ^b Timothy P. Hanusa, ^{a,*} and Tomislav Friščić^{b,*}

Author address:

a) Department of Chemistry, Vanderbilt University, Nashville, TN, 37235, USA; b) Department of Chemistry, McGill University, Montréal, QC, H3A 0B8, Canada

Abstract:

Solid-state mechanochemistry revealed a novel polymorph of the mercury(II) imidazolate framework, based on square-grid (sql) topology layers. Reaction monitoring and periodic density functional theory calculations show that the sql-structure is of higher stability than the previously reported three-dimensional structure, with the unexpected stabilization of a lower dimensionality structure explained by contributions of weak interactions, which include short C-H···Hg contacts.

Main text:

Metal-organic frameworks (MOFs)¹ are one of the most active, prolific areas of materials chemistry, due to a modular design that permits rational incorporation of diverse metal ions and suitably functionalized organic linkers into functional solid-state structures.² While a significant amount of effort has been put into developing materials with improved properties,³ fundamental and systematic studies of how the stability and topology of MOFs are affected by component choice and structure have remained less developed.^{4,5} Popular MOF designs have mostly focused on lighter main group (e.g. Li, 6 Mg, 7 Al8) and first row transition metals 9-13 with the exception of NbOFFIVE, UiO- and NU-type MOFs based on Nb, Zr or Hf. 14-17 Although recent work started exploring the benefits of heavier elements Ce, Th, U or Np¹⁸⁻²⁰ as framework nodes, properties and formation of MOFs with heavier, 6th period members of the periodic table remains largely unexplored.²¹ Consequently, it is unknown to what extent such heavy elements are compatible with, and can bring novelty to, MOF designs. This is particularly relevant for topologically-flexible MOFs, such as zeolitic imidazolate frameworks (ZIFs)²² and other metal azolates,²³ that are prone to polymorphism and can adopt a wide range of topologies depending on metal and linker choice.²⁴ Mercury (as Hg²⁺) is particularly suitable for investigating the effect of heavy elements in ZIFs, as it is the heaviest accessible homologue of Zn²⁺, the most extensively used node in ZIF design. ²²⁻²⁴ As ZIFs with Cd²⁺ have also been studied,²⁵ using a Hg²⁺ node offers a unique opportunity to explore MOF formation across an entire series of homologous transition metals. While MOFs of Hg²⁺ are not likely to be of practical value, due to toxicity of mercury, we see studies of such materials as necessary to fully understand the scope and limitations of MOF designs.

To date, there has been one report of a mercury-based imidazolate framework, a diamondoid (*dia*) topology mercury(II) imidazolate Hg(**Im**)₂.^{26,27} The framework is isostructural to its cadmium analogue, both of which were made by precipitation from aqueous solution and structurally characterized from powder X-ray diffraction (PXRD) data (**Fig. 1a**) by Masciocchi *et al.* In 2006, Fernández-Bertrán *et al.* attempted the synthesis of Hg(**Im**)₂ mechanochemically, ^{28,29}

from HgO and imidazole (HIm), and established that manual grinding led to partial formation of a material with hexagonal symmetry, distinct from dia-Hg(Im)₂.

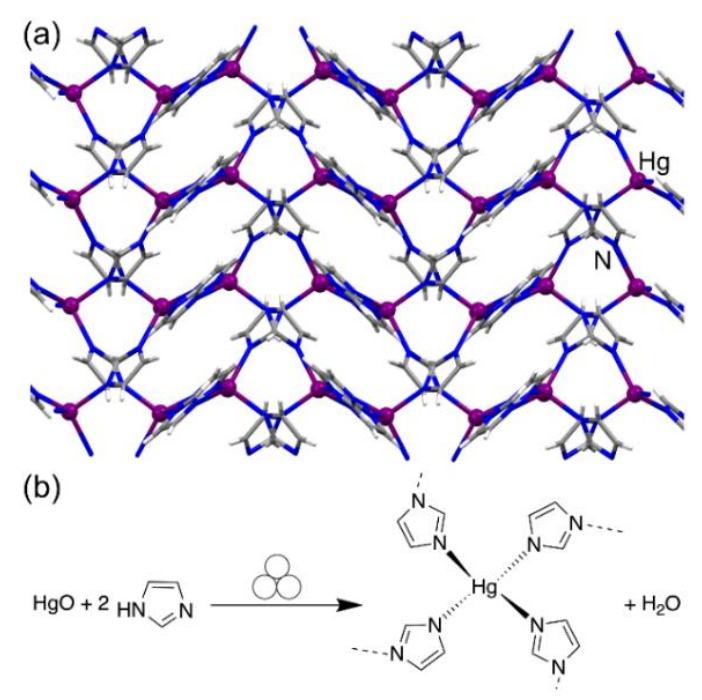


Fig. 1. (a) View of the crystal structure of dia-Hg(\mathbf{Im})₂ and (b) herein explored mechanochemical reaction. The symbol for mechanochemical reaction conditions has been adopted from ref. 28.

Intrigued by this potential difference in mechanochemical and solution-based routes to Hg(Im)₂, we re-investigated the mechanochemical reaction by ball milling HgO and HIm in a respective 1:2 stoichiometric ratio (Fig. 1b),[‡] a methodology previously shown highly successful in making zinc ZIFs.²⁴ Milling was performed in a 25 mL Teflon jar, using one ZrO₂ ball (3.25 grams weight, see ESI). Chemical reaction upon milling was evident by change in color of the reaction mixture from orange (due to HgO) to colorless. After 30 min milling, PXRD analysis revealed complete absence of Bragg reflections of reactants, indicating complete conversion (Fig. 2a). Unexpectedly, the product exhibited X-ray reflections that did not match either the *dia*-Hg(Im)₂ structure or the product of Fernández-Bertrán *et al*.

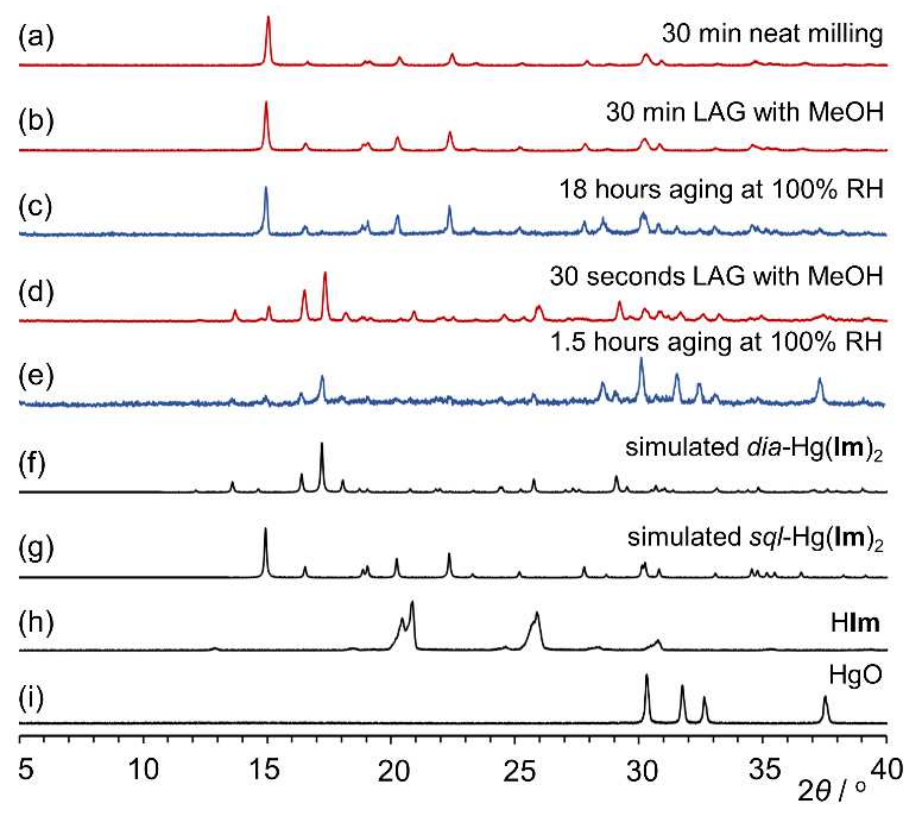


Fig. 2. Comparison of selected PXRD patterns for the reactions of HgO and H**Im**: (a) after 30 min neat milling; (b) after 30 min LAG with MeOH; (c) after 18 h aging at 100% RH; (d) after 30 seconds LAG with MeOH; (e) after 1.5 h aging at 100% RH; (f) simulated for *dia*-Hg(**Im**)₂ (CSD BAYPUN); (g) simulated for *sql*-Hg(**Im**)₂ and measured for: (h) H**Im**; (i) HgO.

The reaction was repeated by liquid-assisted grinding (LAG),³⁰ a method in which the reaction progress is accelerated and directed by small amounts of a liquid. The outcome of the mechanochemical reaction did not change upon LAG with different liquids, including methanol (MeOH, **Fig. 2b**), N,N-dimethylformamide (DMF), acetonitrile (MeCN) or water (see ESI). Thermogravimetric analysis (TGA) of the product revealed no weight loss until the decomposition temperature of ca. 200 °C, indicating that the material does not contain guest solvent.

Attempts to prepare the known dia-Hg(\mathbf{Im})₂ by following the reported solution synthesis were unsuccessful, yielding a microcrystalline powder with a PXRD pattern identical to that of the mechanochemically made material. The PXRD pattern of mechanochemically prepared material was readily indexed to an orthorhombic unit cell in space group $P2_12_12$, with a=9.4089(4) Å, b=7.6414(3) Å, c=5.3625(2) Å, and V=385.55(3) Å³. Structure solution and Rietveld refinement revealed a polymorph of dia-Hg(\mathbf{Im})₂, based on two-dimensional (2D) sheets of composition Hg(\mathbf{Im})₂, with a square-grid (sql) topology ($\mathbf{Fig. 3a,b}$). In contrast to reported dia-Hg(\mathbf{Im})₂, where Hg²⁺ adopts a roughly tetrahedral coordination with N-Hg-N angles from 98.3°-117.7° and Hg-N bonds from 2.18 Å-2.32 Å, the geometry of Hg²⁺ in sql-Hg(\mathbf{Im})₂ is highly distorted, best described as "see-saw" ($\mathbf{Fig. 3c}$).

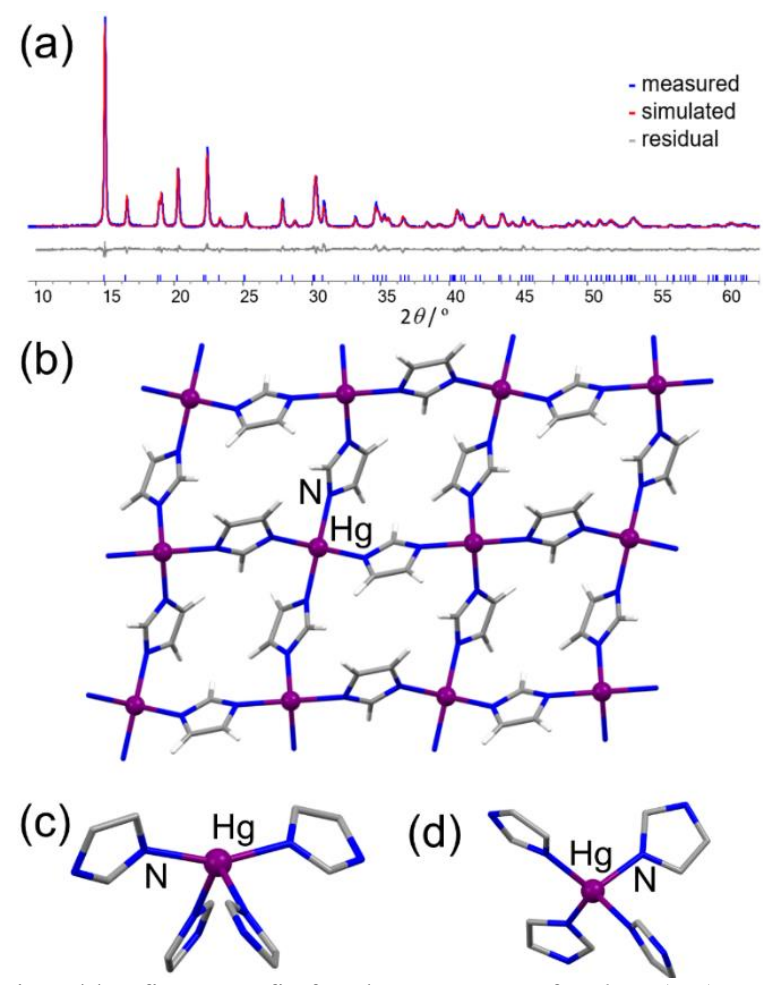


Fig. 3. (a) Final Rietveld refinement fit for the structure of sql-Hg(\mathbf{Im})₂: experimental PXRD pattern is shown in blue, calculated pattern in red, and difference curve in grey. (b) view of a single layer of sql-Hg(\mathbf{Im})₂ along the crystallographic c-axis. Comparison of the coordination geometries of the metal node in: (c) sql-Hg(\mathbf{Im})₂ and (d) dia-Hg(\mathbf{Im})₂, with hydrogen atoms omitted for clarity.

The environment of each Hg²⁺ is defined by two shorter (2.18(2) Å) Hg-N bonds at an angle of 156.1(6)°, and a pair of longer ones (2.31(2) Å), at an angle of 104.6(7)° (**Fig. 3d**). In contrast to other reported *sql*-topology ZIFs Ni(**Im**)₂ (CSD ALIDUU)³¹ and zinc benzimidazolate (CSD KOLYAM),³² where neighboring layers arrange in an offset way, the sheets in *sql*-Hg(**Im**)₂ stack directly on top of each other (see ESI). The coordination of Hg²⁺ in *sql*-Hg(**Im**)₂ is consistent with its ¹⁹⁹Hg solid-state nuclear magnetic resonance (ssNMR) spectroscopy, revealing a powder pattern³³ indicative of axial symmetry, very different from the one seen in *dia*-Cd(**Im**)₂ by ¹¹³Cd ssNMR (see ESI).

We were surprised that all explored mechanochemical and solution-based experiments gave sql-Hg(\mathbf{Im})₂, without any evidence of dia-Hg(\mathbf{Im})₂ or the hexagonal phase reported by Fernández-Bertrán.²⁹ In contrast, the dia-Cd(\mathbf{Im})₂ phase reported by Masciocchi et al. was readily reproduced (see ESI). In an attempt to reproduce any of the reported Hg(\mathbf{Im})₂ phases, we explored a milder synthetic route, by aging³⁴ a 1:2 stoichiometric mixture of HgO and H \mathbf{Im} at 100% relative humidity (RH). Real-time PXRD monitoring³⁵ (**Fig. 4a**) revealed X-ray reflections of dia-Hg(\mathbf{Im})₂

(**Fig. 2e,c**) and Rietveld analysis of the *in situ* data revealed that content of *dia*-Hg(**Im**)₂ increases for ca. 90 minutes, after which it diminishes along with the appearance of *sql*-Hg(**Im**)₂ (**Fig. 4b**). After 140 min, the PXRD pattern exhibits only *sql*-Hg(**Im**)₂.

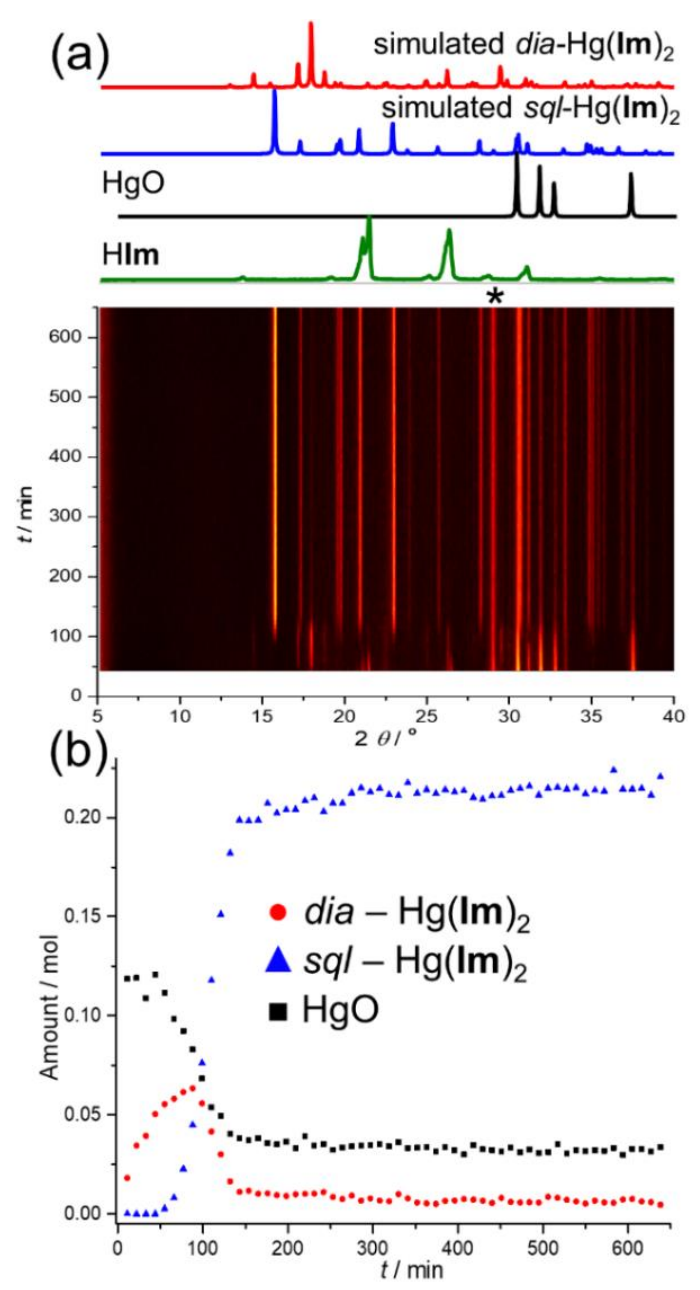


Fig. 4. Real-time monitoring of the aging reaction of HgO and H**Im** by PXRD: (a) time-resolved diffractogram, with diffraction patterns of selected phases shown on top, and Bragg reflection of CeO₂ standard labeled with '*'; (b) reaction profile based on Rietveld fitting, demonstrating changes in amount of HgO, *dia-* and *sql-*Hg(**Im**)₂. Quantitative kinetics analysis was hindered by preferred orientation in the static reaction mixture.

Initial, short-lived appearance of *dia*-Hg(**Im**)₂ in aging led us to explore the milling reaction of HgO and H**Im** at short reaction times. Indeed, PXRD analysis after 30 seconds LAG with MeOH

revealed the appearance of dia-Hg(**Im**)₂ along with unreacted HgO and H**Im** (**Fig. 2d**). After 1 minute, the reaction mixture exhibits only reflections of sql-Hg(**Im**)₂.

Calculated densities of dia- and sql-Hg(\mathbf{Im})₂ are remarkably similar, preventing the deduction of relative stabilities. However, the dia-Hg(\mathbf{Im})₂ $\rightarrow sql$ -Hg(\mathbf{Im})₂ transformation in aging and milling indicates that sql-form should be the thermodynamically more stable phase. ²⁴ This was validated by periodic density functional theory (DFT) calculations, performed in periodic DFT code CRYSTAL17³⁶ using the hybrid B3LYP³⁷ functional combined with the Grimme D3 semiempirical dispersion correction, ³⁸ which showed that the sql-form is 10.21 kJ mol⁻¹ lower in energy than the dia-one. This contrasts Zn(\mathbf{Im})₂³⁹ and Cd(\mathbf{Im})₂, whose most stable forms exhibit three-dimensional (3D) zni- and dia-topologies, respectively.

Intrigued by the unexpected difference between our study and previous reports on $Hg(\mathbf{Im})_2$, we performed similar calculations for the reported dia-Cd(\mathbf{Im})₂ and the hypothetical sql-Cd(\mathbf{Im})₂ structure obtained by DFT optimization of a model obtained by replacing all Hg atoms in sql-Hg(\mathbf{Im})₂ with Cd. In this case, the two structures were found to have very similar energies, sql-Cd(\mathbf{Im})₂ being just 0.39 kJ mol⁻¹ more stable. The improved stability of the dia-structure in Cd(\mathbf{Im})₂ is consistent with numerous experimental observations of dia-Cd(\mathbf{Im})₂.

Stabilization of the 2D sql-structure in $Hg(\mathbf{Im})_2$ compared to a more extensively connected and interpenetrated 3D dia-framework is unexpected and, we believe, associated to weak intermolecular interactions between layers. This is consistent with calculations of relative stabilities of dia- and sql-Hg(Im)2 using the B3LYP functional uncorrected for dispersion. Under such conditions, stabilities of the two structures are inverted, with the dia-form becoming 7.81 kJ mol^{-1} more stable. Whereas the sql-Hg(\mathbf{Im})₂ structure reveals short contacts between neighboring layers, readily interpreted as C-H \cdots π and π \cdots π interactions, it also exhibits a short H \cdots Hg contact of 3.26(3) Å, not present in the dia-form. Most proposed van der Waals radii for Hg range from 2.00 to 2.53 Å, 40 indicating that this contact might be up to 9% shorter than the sum of van der Waals radii of hydrogen (1.25 Å) and mercury. The unique appearance and energetic stability of sql-Hg(Im)2, as opposed to its hypothetical sql-Cd(Im)2 analogue, led us to perform Bader's quantum theory of atoms in molecules (QTAIM)⁴¹ analysis on the DFT-optimized structures, searching for bond critical points (BCPs) as evidence for structure-stabilizing interactions. The sql-Hg(Im)₂ and Cd(Im)₂ structures display a very similar distribution of non-covalent BCPs (see ESI), with the exception of one BCP in the vicinity of the Hg atom. This critical point, unique to sql-Hg(Im)₂, reveals a moderate bonding interaction (0.074 electrons \mathring{A}^{-3}) between the metal atom and the C-H bond of an imidazolate linker from an adjacent metal-organic layer. This BCP is coincident with the experimentally noted short H···Hg contact, suggesting its importance for the overall stabilization of sql-Hg(Im)₂. While this H···Hg contact cannot be interpreted as a conventional bond, it is clearly stabilizing, tentatively corresponding to a weak agostic bond.⁴²

In summary, a re-investigation of an early report of mechanochemical MOF formation has revealed a novel, layered polymorph of a so far unique mercury(II) imidazolate framework. Experiment and theory indicate that the layered polymorph is thermodynamically more stable than the previously reported interpenetrated *dia*-framework, evidently due to weak intermolecular forces that include previously unreported intermolecular agostic-like C-H····Hg contacts. Such stabilization of a layered structure makes a striking contrast between Hg²⁺ and its congeners Cd²⁺ and Zn²⁺, whose imidazolates in their most stable form favor 3D frameworks, highlighting the potential for differences in MOF formation when using a heavy element compared to its lighter congeners.

Conflicts of interest

There are no conflicts of interest to declare.

Acknowledgements

IRS and TPH acknowledge financial support by the NSF (CHE-1665327) and ACS-PRF (56027-ND3); TF acknowledges support of NSERC (RGPIN-2017-06467, STPGP 521582-18). We thank Prof. R. W. Schurko (National MagLab) and Dr. V. Zorin (JEOL) for help setting up the BRAIN-CP/WURST-CPMG pulse sequences.

Notes

[‡]Mercury compounds are highly toxic, and all operations must be conducted with great care and precaution.

References:

- 1 a) S. R. Batten, N. R. Champness, X.-M. Chen, J. Garcia-Martinez, S. Kitagawa, L. Öhrstrom, M. O'Keeffe, M. Paik Suh and J. Reedijk *CrystEngComm* 2012, **14**, 3001.
- 2 a) B. Rungtaweevoranit, C. S. Diercks, M. J. Kalmutzki and O. M. Yaghi *Faraday Discuss*. 2017, **201**, 9; b) P. Deria, J. E. Mondloch, O. Karagiaridi, W. Bury, J. T. Hupp and O. K. Farha *Chem. Soc. Rev.* 2014, **43**, 5896.
- 3 a) H. Furukawa, N. Ko, Y. B. Go, N. Aratani, S. B. Choi, E. Choi, A. Ö. Yazaydin, R. Q. Snurr, M. O'Keeffe, J. Kim and O. M. Yaghi *Science* 2010, **329**, 424; b) M. F. de Lange, K.
- J. F. M. Verouden, T. J. H. Vlugt, J. Gascon and F. Kapteijn Chem. Rev. 2015, 115, 12205.
- 4 a) M. E. Schweinefuß, S. Springer, I. A. Baburin, T. Hikov, K. Huber, S. Leoni and M. Wiebcke *Dalton Trans.* 2014, 43, 3528; b) F.-X. Coudert, A. H. Fuchs *Coord. Chem. Rev.* 2016, 307, 211.
- 5 a) M. Arhangelskis, A. D. Katsenis, A. J. Morris and T. Friščić *Chem. Sci.* 2018, **9**, 3367; b) H. M. Titi, M. Arhangelskis, A. D. Katsenis, C. Mottillo, G. Ayoub, J.-L. Do, A. M. Fidelli, R. D. Rogers and T. Friščić *Chem. Mater.* 2019, **31**, 4882.
- 6 J. Zhang, T. Wu, C. Zhou, S. Chen, P. Feng and X. Bu *Angew. Chem. Int. Ed.* 2009, **48**, 2542.
- 7 D. Gygi, E. D. Bloch, J. A. Mason, M. R. Hudson, M. I. Gonzalez, R. L. Siegelman, T.
- A. Darwish, W. L. Queen, C. M. Brown and J. R. Long *Chem. Mater.* 2016, **28**, 1128.
- 8 T. Loiseau, C. Serre, C. Huguenard, G. Fink, F. Taulelle, M. Henry, H. Bataille and G. Férey *Chem. Eur. J.* 2004, **10**, 1373.
- 9 G. Férey, C. Mellot-Draznieks, C. Serre, F. Millange, J. Dutour, S. Surblé and I. Marhiolaki *Science* 2005, **309**, 2040.
- 10 J. López-Cabrelles, J. Romero, G. Abellán, M. Giménez-Marqués, M. Polomino, S. Valencia, F. Rey and G. Mínguez Espallargas *J. Am. Chem. Soc.* 2019, **141**, 7173.
- 11 H. Deng, S. Grunder, K. E. Cordova, C. Valente, H. Furukawa, M. Hmadeh, F. Gándara, A. C. Whalley, Z. Liu, S. Asahina, H. Kazumori, M. O'Keeffe, O. Terasaki, J. F. Stoddart
- and O. M. Yaghi *Science* 2012, **336**, 1018.
- 12 G. Zhong, D. Liu and J. Zhang J. Mat. Chem. A 2018, 6, 1887.
- 13 S. S.-Y. Chui, S. M.-F. Lo, J. P. H. Charmant, A. G. Orpen and I. D. Williams *Science* 1999, **283**, 1148.
- 14 P. M. Bhatt, Y. Belmabkhout, A. Cadiau, K. Adil, O. Shekhah. A. Shkurenko, L. J. Barbour and M. Eddaoudi *J. Am. Chem. Soc.* 2016, **138**, 9301.

- 15 J. Hafizovic-Cavka, S. Jakobsen, U. Olsbye, N. Guillou, C. Lamberti, S. Bordiga and K. P. Lillerud, *J. Am. Chem. Soc.* 2008, **130**, 13850.
- 16 T. C. Wang, N. A. Vermeulen, I. S. Kim, A. B. F. Martinson, J. F. Stoddart, J. T. Hupp, O. K. Farha *Nat. Prot.* 2016, **11**, 149.
- 17 M. J. Cliffe, W. Wan, X. Zou, P. A. Chater, A. K. Kleppe, M. G. Tucker, H. Wilhelm, N. P. Funnell, F.-X. Coudert and A. L. Goodwin *Nat. Commun.* 2014, **5**:4176.
- 18 M. Lammert, M. T. Wharmby, S. Smolders, B. Bueken, A. Lieb, K. A. Lomachenko, D. De Vos and N. Stock *Chem. Commun.* 2015, **51**, 12578.
- 19 a) K. P. Carter, J. A. Ridenour, M. Kalaj and C. L. Cahill *Chem. Eur. J.* 2019, **25**, 7114;
- b) E. A. Dolgopolova, A. M. Rice and N. B. Shustova *Chem. Commun.* 2018, **54**, 6472.
- 20a) C. Falaise, C. Volkringer, J.-F. Vigier, N. Henry, A. Beaurain and T. Loiseau *Chem.*
- *Eur. J.* 2013, **19**, 5324; b) S. E. Gilson, P. Li, J. E. S. Szymanowski, J. White, D. Ray, L. Gagliardi, O. K. Farha and P. C. Burns *J. Am. Chem. Soc.* 2019, **141**, 11842.
- 21 a) Y. Zhang, B. E. G. Lucier, S. M. McKenzie, M. Arhangelskis, A. J. Morris, T. Friščić,
- J. W. Reid, V. V. Terskikh, M. Chen and Y. Huang ACS Appl. Mater. Int. 2018, 10, 28582;
- b) L. Robison, L. Zhang, R. J. Drout, P. Li, C. R. Haney, A. Brikha, H. Noh, B. L. Mehdi,
- N. D. Browning, V. P. Dravid, Q. Cui, T. Islamoglu and O. K. Farha *ACS Appl. Biomat.* 2019, **2**, 1197.
- 22 K. S. Park, Z. Ni, A. P. Côte, J. Y. Choi, R. Huang, F. J. Uribe-Romo, H. K. Chae, M. O'Keeffe and O. M. Yaghi *Proc. Natl. Acad. Sci. U.S.A.* 2006, **103**, 10186.
- 23 J.-P. Zhang, Y.-B. Zhang, J.-B. Lin and X.-M. Chen Chem. Rev. 2012, 112, 1001.
- 24 a) Z. Akimbekov, A. D. Katsenis, G. P. Nagabushana, G. Ayoub, M. Arhangelskis, A. J. Morris, T. Friščić and A. Navrotsky *J. Am. Chem. Soc.* 2017, **139**, 7952; b) M.
- Arhangelskis, A. D. Katsenis, N. Novendra, Z. Akimbekov, D. Gandrath, J. M. Marrett, G. Ayoub, A. J. Morris, O. K. Farha, T. Friščić and A. Navrotsky *Chem. Mater.* 2019, **31**, 3777.
- 25 a) Y.-Q. Tian, S.-Y. Yao, D. Gu, K.-H. Cui, D.-W. Guo, G. Zhang, Z.-X. Chen and D.-Y. Zhao, *Chem. Eur. J.* 2010, **16**, 1137; b) S.-Y. Yao and Y.-Q. Tian *CrystEngComm* 2010, **12**, 697.
- 26 N. Masciocchi, G. A. Ardizzoia, S. Brenna, F. Castelli, S. Galli, A. Maspero and A. Sironi, *Chem. Commun.* 2003, 2018.
- 27 A search of the Cambridge Structural Database (CSD version 5.40, Feb 2019 update) also reveals two Hg(II) tetrazolate frameworks, and a pyrazolate: a) D.-S. Liu, Y. Sui, G.-M. Ye,
- H.-y. Wang, J.-Q. Liu and W.-T. Chen *J. Solid State Chem.* 2018, **263**, 182; b) J. Xianglin, S. Meicheng, H. Haochuan, W. Jinming and Z. Yu *Chin. Chem. Bull.* 1982, 336; c) N.
- Masciocchi, G. A. Ardizzoia, A. Maspero, G. LaMonica and A. Sironi *Inorg. Chem.* 1999, **38**, 3657.
- 28 N. R. Rightmire, T. P. Hanusa *Dalton Trans.* 2016, **45**, 2352.
- 29 J. F. Fernández-Bertran, M. P. Hernández, E. Reguera, H. Yee-Madeira, J. Rodriguez, A. Paneque and J. C. Llopiz *J. Phys. Chem. Sol.* 2006, **67**, 1612.
- 30 T. Friščić, C. Mottillo and H. M. Titi *Angew. Chem. Int. Ed.* 2019, DOI:10.1002/anie.201906755
- 31 N. Masciocchi, F. Castelli, P. M. Forster, M. M. Tafoya and A. K. Cheetham *Inorg. Chem.* 2003, **42**, 6147.
- 32 Q.-F. Yang, X.-B. Cui, J.-H. Yu, J. Lu, X.-Y. Yu, X. Zhang, J.-Q. Xu, Q. Hou and T.-G. Wang *CrystEngComm* 2008, **10**, 1531.

- 33 K. J. Harris, A. Lupulescu, B. E. G. Lucier, L. Frydman and R. W. Schurko, *J. Magn. Reson.* 2012, **224**, 38.
- 34 C. Mottillo and T. Friščić Molecules 2017, 22, 144.
- 35 I. Huskić, J.-C. Christopherson, K. Užarević and T. Friščić *Chem. Commun.* 2016, **52**, 5120.
- 36 R. Dovesi, A. Erba, R. Orlando, C. M. Zicovich-Wilson, B. Civalleri, L. Maschio, M. Rérat, S. Casassa, J. Baima, S. Salustro and B. Kirtman, *Wiley Interdiscip. Rev. Comput. Mol. Sci.*, 2018, **8**, e1360
- 37 a) A. D. Becke, *J. Chem. Phys.*, 1993, **98**, 5648; b) C. Lee, W. Yang and R. G. Parr, *Phs. Rev. B*, 1988, **37**, 785
- 38 S. Grimme, J. Antony, S. Ehrlich and H. Krieg, *J. Chem. Phys.*, 2010, **132**, 154104.
- 39 I. A. Baburin, S. Leoni and G. Seifert J. Phys. Chem. B 2008, 112, 9437.
- 40a) S.-Z. Hu, Z.-H. Zhou and B. E. Robertson *Z. Kristallogr.* 2009, **224**, 375; b) S. Alvarez *Dalton Trans.* 2013, **42**, 8617.
- 41 R. F. W. Bader, J. Phys. Chem. A, 1998, 102, 7314.
- 42 Y.-C. Chen, J.-Y. Tung, T.-K. Liu, W.-J. Tsai, H.-Y. Lin, Y.-C. Chang and J.-H. Chen *Dalton Trans.* 2018, **47**, 14774.

Supplementary Information

Mechanochemical synthesis of a mercury(II) metal-organic framework reveals a two-dimensional polymorph stabilized by weak interactions

I. R. Speight ^a, I. Huskić ^b, M. Arhangelskis ^b, H. M. Titi ^b, R. S. Stein ^b, T. P. Hanusa *a, T. Friščić *b

^aDepartment of Chemistry, Vanderbilt University, Nashville, Tennessee, USA, 37235; ^bDepartment of Chemistry, McGill University, Montreal, H3A 0B8, Canada

Corresponding authors:

*Prof. Tomislav Friščić, E-mail: tomislav.friscic@mcgill.ca

*Prof. Timothy P. Hanusa, E-mail: t.hanusa@vanderbilt.edu

Table of Contents

• Please note that all theoretically generated structures, as well as experimentally determined crystal structures, have been provided as CIF files

S.	1 N	MATERIALS AND METHODS	. 2
	S.1.1	Thermal analysis	.2
	S.1.2	Powder X-ray diffraction	. 2
	S.1.3	Structure determination from powder X-ray data	. 2
	S.1.4	Solid-state nuclear magnetic resonance (NMR) spectroscopy	.3
	S.1.5	Fourier-transform infrared attenuated total reflectance (FTIR-ATR) spectroscopy	. 4
S.	2 S	YNTHETIC PROCEDURES	.4
	S.2.1	Abbreviations	.4
	S.2.2	Synthesis of the <i>sql</i> -Hg(Im) ₂ framework by milling	.4
	S.2.3	Synthesis of the dia–Hg(Im) ₂ framework by milling	.4
	S.2.4	Synthesis of the sql-Hg(Im) ₂ framework from solution	.4
	S.2.5	In situ monitoring of Hg(Im)2 framework synthesis by aging	.4
	S.2.6	Synthesis of dia-Cd(Im)2 framework from solution	. 5
	S.2.7	Synthesis of zni-Zn(Im) ₂ framework by milling	. 5
S.	3 (COMPUTATIONAL METHODS	. 5
	S.3.1	Geometry optimization	. 5

S.3.	.2 Bader analysis	5
S.4	X-ray diffraction	7
S.4	.1 Powder X-ray diffraction patterns	7
S.4	.2 Rietveld refinement of <i>sql</i> -Hg(Im) ₂ structure	10
S.5	Thermogravimetric analysis (TGA) of prepared materials	12
S.6	Fourier-transform infrared attenuated total reflectance (FTIR-ATR) spectra	13
S.7	Solid-state NMR spectroscopy	14
S.8	Bader Analysis	16
S.9	Comparison to Other 2-D ZIF Structures	18
S.10	References	19

S.1 MATERIALS AND METHODS

HgO (≥99%) and imidazole (HIm) (≥99%) were purchased from Aldrich. Methanol (MeOH), N,N-dimethylformamide (DMF), and acetonitrile (MeCN) were purchased from ACP Chemicals. All chemicals were used without further purification. Mercury compounds should be treated with rigorous safety precautions due to their toxicity. Care was taken at all times to avoid contact with solid, solution, and air-borne particulate mercury compounds. All reactions, equipment, and waste were treated and disposed of properly.

S.1.1 Thermal analysis

Thermogravimetric analyses (TGA) were performed utilizing 2 mg of sample on a TGA/DSC 1 system with a sulfur trap attached to avoid release of mercury vapors to the open atmosphere. The system was operated on a PC with STAR^e software. Samples were heated from 25 to 600 °C at a rate of 10 °C/min under flowing air. The balance and purge flow were 40 mL/min and 25 mL/min respectively.

S.1.2 Powder X-ray diffraction

Powder X-ray diffraction (PXRD) patterns were collected using a Bruker D2 Phaser powder diffractometer equipped with a Cu- $K\alpha$ ($\lambda = 1.5418$ Å) source and Lynxeye detector. The patterns were collected in the angle region between 4° and 40° (2θ) with a step size of 0.05°. PXRD patterns used for structure solution-refinement were collected in the angle region between 4° and 70° (2θ) with a step size of 0.02° and 6.0 s counting per step.

S.1.3 Structure determination from powder X-ray data

The PXRD pattern of sql-Hg(**Im**)₂ was indexed using the DASH 3.4.2 program suite¹ and the DICVOL06 algorithm,² giving the following unit cell with orthorhombic metric symmetry: a = 9.41 Å, b = 7.64 Å, c = 5.36 Å ($V = 385.3 \text{ Å}^3$). The space group was assigned as $P2_12_12_2$. From consideration of the density and volume of the unit cell, there are two formula units of HgIm₂ (Z = 2) in the unit cell. Profile fitting using the Pawley method³ in the TOPAS6⁴ program gave a reasonable quality of fit ($R_p = 5.74\%$, $R_{wp} = 8.69\%$), and refined unit cell parameters of

a = 9.4089(4) Å, b = 7.6414(3) Å and c = 5.3625(2) Å. The refined unit cell parameters were used in the subsequent structure-solution calculation.

Structure solution was carried out using the simulated annealing technique in the program DASH 3.4.2. The crystal structure was defined by 9 variables: six variables for the imidazolate fragment (three positional variables and three orientational variables), and three positional variables for the Hg⁺² cation.

The structure solution was then used as the starting model for Rietveld refinement, 5 carried out in TOPAS6 program. In the Rietveld refinement, standard restraints were applied to bond lengths and bond angles, and planar restraints were applied to the imidazolate group. The final Rietveld refinement gave a reasonable fit to the powder XRD data ($R_p = 7.09\%$, $R_{wp} = 9.22\%$).

S.1.4 Solid-state nuclear magnetic resonance (NMR) spectroscopy

All MAS spectra and the static ¹¹³Cd powder pattern were acquired on a Varian VNMRS (now Agilent, Santa Clara, CA, USA) spectrometer operating at 399.8 MHz for ¹H, 100.5 MHz for ¹³C, 89.5 MHz for ¹⁹⁹Hg, 88.7 MHz for ¹¹³Cd, and 40.5 MHz for ¹⁵N using a 4 mm double-resonance Varian Chemagnetics T3 probe (now Agilent, Santa Clara, CA, USA). Approximately 70 mg of sample were center-packed into rotors using either Teflon or boron nitride inserts, and spun at between 8 and 15 kHz for MAS. The static ¹⁹⁹Hg spectrum of *sql*-Hg(**Im**)₂ was acquired on a Varian VNMRS spectrometer operating at 499.9 MHz for ¹H and 89.5 MHz for ¹⁹⁹Hg using a 6 mm double-resonance Varian Chemagnetics T3 probe.

The ¹³C CPMAS spectrum was acquired in 512 scans under spinning at 8 kHz, using a recycle delay of 10 s with a contact time of 4 ms at a ¹³C rf field of approximately 60 kHz. SPINAL-64 decoupling at an rf field of 90 kHz was applied during acquisition. Spectra were referenced using the carbonyl carbon signal in glycine at 176.4 ppm with respect to TMS.⁶

The ¹⁵N CPMAS spectrum of *sql*-Hg(**Im**)₂ was acquired under spinning at 8 kHz in 7260 scans, with a contact time of 3 ms at a ¹⁵N rf field of approximately 45 kHz. The recycle delay was 10 s. SPINAL-64 decoupling at an rf field of 70 kHz was applied during acquisition. Spectra were referenced using the nitrogen signal in glycine at 33.4 ppm with respect to liquid ammonia.⁷

The 199 Hg BRAIN-CP/WURST-CPMG⁸ spectrum of sql-Hg(**Im**)₂ was acquired in 896 scans using a recycle delay of 8 s. A 4 µs (62.5 kHz) π /2 excitation pulse was used on the 1 H channel and 40 kHz of spin-locking power was applied on both channels for the optimized contact time. The WURST spin-locking pulse of 199 Hg was swept over 400 kHz in 6000 points. The CPMG refocusing portion of the sequence used 50 µs WURST-80 pulses, with ν_1 = 35 kHz and 800 kHz sweep ranges. The spectral width was 500 kHz (2 µs dwell time). The acquisition period of a single echo was 0.56 ms and 29 echoes were acquired in each scan. All 199 Hg spectra were referenced using the isotropic 199 Hg chemical shift of mercuric acetate at -2495 ppm with respect to Hg(CH₃)₂.

Two ¹⁹⁹Hg CPMAS spectra (not shown) were acquired of *sql*-Hg(**Im**)₂, one under spinning at 8 kHz (768 scans) and the other spinning at 10 kHz (2048 scans). In both, a contact time of 8 ms was used at a ¹⁹⁹Hg rf field of approximately 50 kHz. SPINAL-64 decoupling at an rf field of 90 kHz was applied during acquisition and the recycle delay was 5 s.

The 113 Cd static spectrum of dia-Cd(**Im**)₂was acquired using cross-polarization at an rf field of approximately 50 kHz in 6144 scans using a 5 s recycle delay. Spectra were referenced to Cd(NO₃)₂ at -102.2 ppm with respect to Cd(ClO₄)₂·6H₂O.¹⁰

¹H single-pulse spectra were acquired with spinning at 15 kHz and were referenced to adamantane at 1.87 ppm¹¹ with respect to TMS. High resolution ¹H spectra were acquired using the windowed PMLG-5¹² sequence with 100 kHz rf (16.3 μs pulses and 1 μs acquisition) for a total of 10 ms acquisition in 4 scans (recycle delay of 4 s). The PMLG spectra were referenced

and scaled using a spectrum of α -glycine whose signals were referenced to 8.4 ppm and 3.4 ppm (the center of the CH₂ signals) with respect to TMS.¹³

S.1.5 Fourier-transform infrared attenuated total reflectance (FTIR-ATR) spectroscopy

Infrared spectra were obtained using using a Bruker Alpha FT-IR spectrometer (Bruker Optics Ltd., Milton, ON, Canada) decorated by diamond crystal in the range of 4000-450 cm⁻¹ and with resolution of 4 cm⁻¹, and are reported in wavenumber (cm⁻¹) units for the most significant absorption bands.

S.2 SYNTHETIC PROCEDURES

For mechanochemical experiments, reactions were conducted in a Teflon milling jar of 25 mL volume, using one 7 mm diameter (weight ~3.2 grams) zirconia ball, and either a Retsch MM400 or Retsch MM200 mill operating at 25 Hz. All samples of metal-organic frameworks were used without further treatment.

S.2.1 Abbreviations

HIm = 1H-imidazole; BzIm = 1-Benzylimidazole; MeOH = methanol; DMF = N,N-dimethylformamide; MeCN = acetonitrile.

S.2.2 Synthesis of the sql-Hg(Im)₂ framework by milling

A solid mixture of HgO (108.3 mg, 0.50 mmol) and HIm (68.1 mg, 1.00 mmol, 1:2 stoichiometric ratio with respect to total mercury content) were placed in a 25 mL Teflon jar along with either 50 μ L of MeOH, MeCN, DMF, or no additive, and the reaction mixture was milled for a period of 30 minutes. The material was analyzed without further treatment.

S.2.3 Synthesis of the dia-Hg(Im)₂ framework by milling

A solid mixture of HgO (108.3 mg, 0.50 mmol) and HIm (68.1 mg, 1.00 mmol, 1:2 stoichiometric ratio with respect to total mercury content) were placed in a 25 mL Teflon jar along with 50 μ L of MeOH and the reaction mixture was milled for 30 seconds. The reaction mixture after milling contained small amounts of HgO. Attempts to remove residual HgO with longer milling times, addition of a catalyst salt, or change of liquid additive all led to the formation of either a mixture of the *dia*- and *sql*-Hg(Im)₂ frameworks or the *sql*-Hg(Im)₂ framework solely.

S.2.4 Synthesis of the sql-Hg(Im)₂ framework from solution

A 250 mL round bottom flask was charged with a Teflon stirring bar, mercury(II) acetate (5.00 g, 15.7 mmol, 1 equiv.), and HIm (4.25 g, 62.4 mmol, 4 equiv.). Next, 100 mL of de-ionized water was added to the flask and the solution was stirred. Aqueous ammonia (28% v/v) (7.01 mL, 68.1 mmol) was added slowly down the side of the flask. The reaction was allowed to stir at ambient temperature for 3 h. The reaction was then filtered and the isolated material was washed twice with 25 mL portions of de-ionized water, washed once with 25 mL of methanol and then dried.

S.2.5 In situ monitoring of Hg(Im)₂ framework synthesis by aging

A sample of HgO (108.3 mg, 0.50 mmol, 1 equiv.) and HIm (68.1 mg, 1.00 mmol, 2 equiv.) were ground separately in a mortar and pestle. The two solids were placed in a vial along with CeO₂ (17.6 mg, 10% w/w) as an internal X-ray diffraction standard. The mixture was agitated

in a vial to create a homogenous mixture. A small portion of the mixture was then transferred to a custom designed PXRD sample holder with two grooves ground into the surface. In each groove of the customized sample holder was placed 200 μ L of water to act as a source of humidity. The holder was then covered with a small sheet of Saran wrap, in order to seal the chamber and generate a saturated humidity atmosphere. Samples were aged under such humid atmosphere for a period of 17.5 hours, with powder X-ray diffraction patterns recorded periodically every 11 minutes and 24 seconds.

S.2.6 Synthesis of dia-Cd(Im)₂ framework from solution

A solution of Cd(NO₃)₂ (500.0 mg, 2.12 mmol) in 17 mL of MeOH was added to a 100 mL round bottom flask equipped with a Teflon stirring bar. To the stirring solution, H**Im** (288.7 mg, 4.24 mmol, 2 equiv.) dissolved in 7 mL of MeOH was added all at once. NaOH (169.5 mg, 4.24 mmol) was dissolved in 1 mL of deionized water and added dropwise to the stirring solution. After 5 minutes of stirring, a white precipitate formed. The reaction was vacuum filtered and the filtrate was washed twice with 10 mL portions of methanol and twice with 10 mL portions of deionized water. To ensure its dryness, the product was placed in a 45 °C oven for 30 minutes. The product was identified by its characteristic PXRD pattern.

S.2.7 Synthesis of zni-Zn(Im)₂ framework by milling

A solid mixture of ZnO (75.0 mg, 0.94 mmol) and HIm (123.0 mg, 1.80 mmol, 2 equiv.) were placed in a 25mL Teflon milling jar with 2 zirconia balls (\sim 3.25 g/ball) and 100 μ L of MeOH. The reaction was milled at 30 Hz for one hour to give a white free flowing powder. The material was analyzed without further treatment and identified from its characteristic PXRD pattern.

S.3 COMPUTATIONAL METHODS

S.3.1 Geometry optimization

The *dia*- and *sql*- structures of $Hg(Im)_2$ and $Cd(Im)_2$ were geometry-optimized using the periodic DFT code CRYSTAL17¹⁵ using the hybrid B3LYP^{16,17} functional supplemented with the Grimme D3¹⁸ semiempirical dispersion correction. The wavefunctions were constructed using the POB-TZVP basis set (H, C, N, Cd)^{119,20} and a double-zeta basis set for $Hg.^{21}$ Effective core potentials (ECPs) were used for Cd and Hg atoms.²² The electronic 1st Brillouin zone was sampled with a 0.05 Å-¹ Monkhorst-Pack k-point spacing. Crystal structures were optimized with respect to atom coordinates and unit cell parameters, subject to the symmetry constraints of their respective space groups. The following convergence criteria were used for geometry optimization: maximum force on atom $4.5 \cdot 10^{-4}$ Ha Bohr⁻¹, RMS force $3.0 \cdot 10^{-4}$ Ha Bohr⁻¹, maximum atom displacement $1.8 \cdot 10^{-3}$ Bohr, RMS atom displacement $1.2 \cdot 10^{-3}$ Bohr. The energies of all crystal structures were corrected for basis set superposition error (BSSE) using the counterpoise method with ghost atoms located up to 5 Å away from the reference molecule.

S.3.2 Bader analysis

Topological analysis of the calculated electron density for the optimized sql structures of $Hg(\mathbf{Im})_2$ and $Cd(\mathbf{Im})_2$ was performed using the TOPOND program accessed through the CRYSTAL Properties module. In the case of $Hg(\mathbf{Im})_2$, the electron density obtained from the

final geometry optimization step was used in the analysis. For Cd(**Im**)₂ a single point calculation using a double zeta basis set for Cd atom was performed.²³ This was necessary, as the *f*-functions in the original POB_TZVP basis set for Cd could not be processed by the TOPOND code. Critical points were searched using an automated eigenvector following algorithm. The contour electron density and Laplacian contour plots (Figures S23-24) were drawn with the aid of the CRYSPLOT visualization tool.

S.4 X-ray diffraction

S.4.1 Powder X-ray diffraction patterns

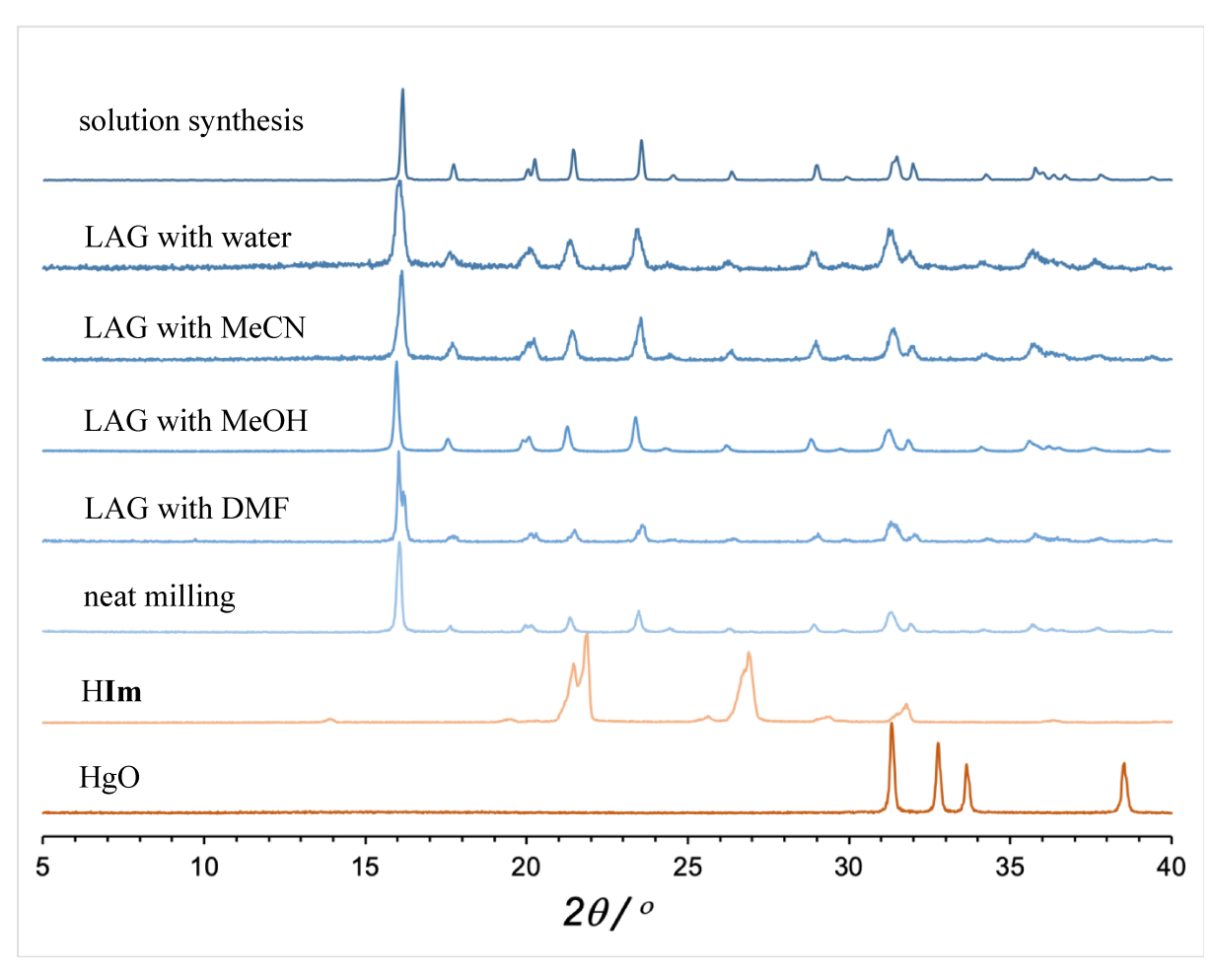


Figure S1. Selected PXRD patterns for $Hg(Im)_2$ product obtained from solution synthesis or by mechanochemical reaction of **1 HgO + 2** HIm by neat milling or LAG with different solvent additives. All milling reactions were performed in a 25 mL Teflon jar using one 7 mm diameter (3.2 g weight) zirconia ball, and either a Retsch MM400 or MM200 mill operating at 25 Hz for 30 minutes. For LAG reactions, 50 μ L of a liquid phase were added to the reaction mixture.

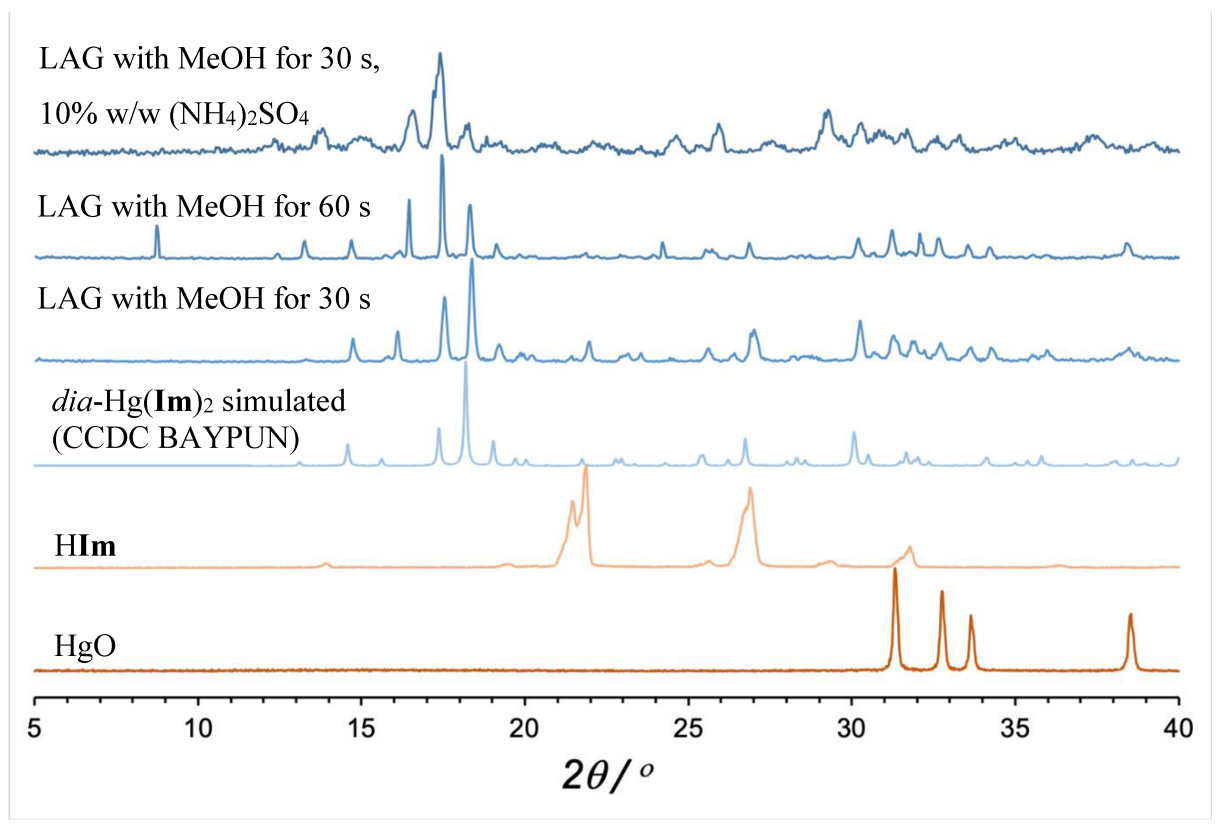


Figure S1. Selected PXRD patterns for attempts of mechanochemical synthesis of dia-Hg(Im)₂ by LAG. All reactions were performed in a 25 mL Teflon jar using one 7 mm diameter (3.2 g weight) zirconia ball, and a Retsch MM400 or MM200 mill operating at 25 Hz. In all reaction 50 μ L of MeOH was added.

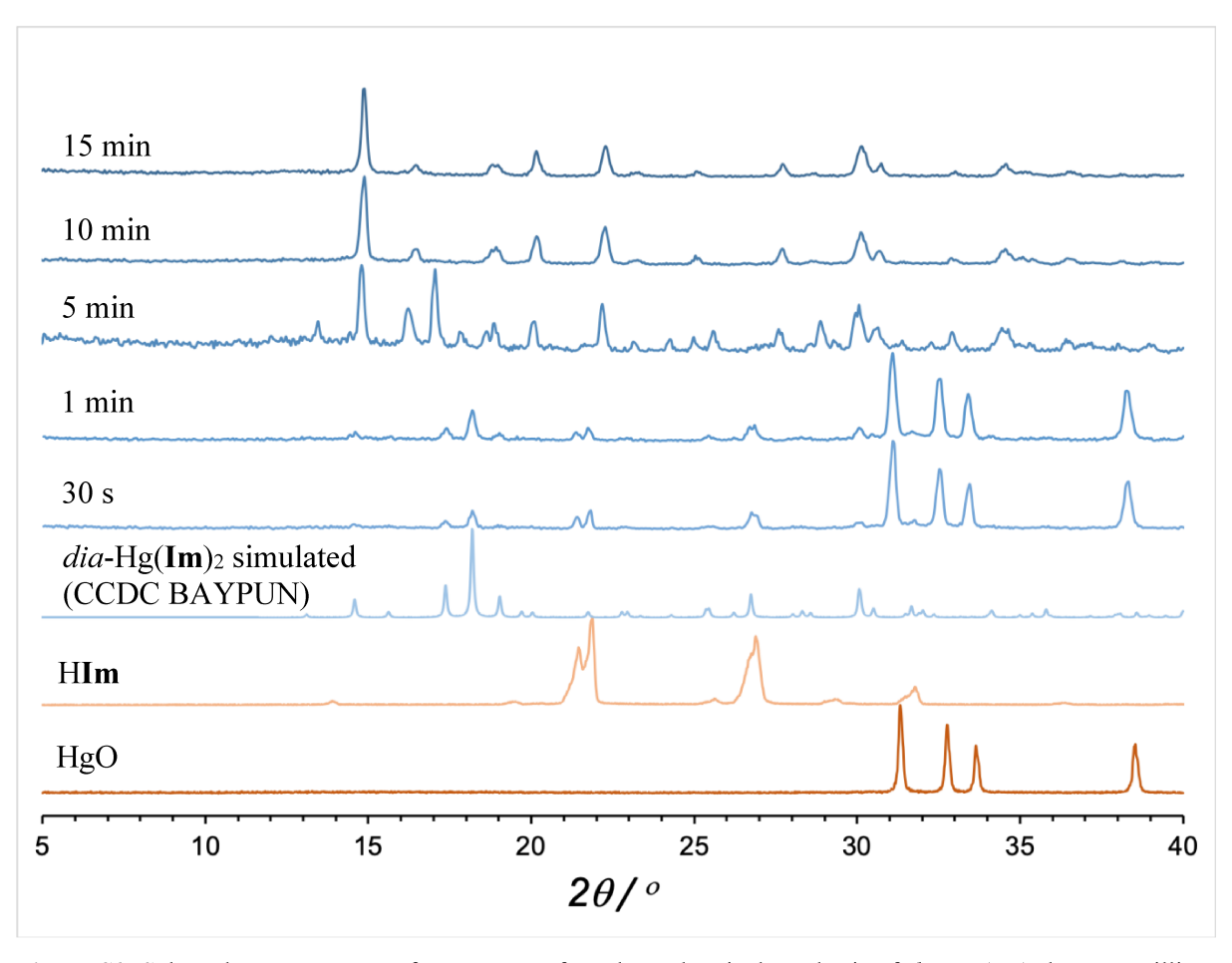


Figure S3. Selected PXRD patterns for attempts of mechanochemical synthesis of dia-Hg(Im)₂ by neat milling. All reactions were performed in a 25 mL Teflon jar using one 7 mm diameter (3.2 g weight) zirconia ball, and a Retsch MM400 or MM200 mill operating at 25 Hz.

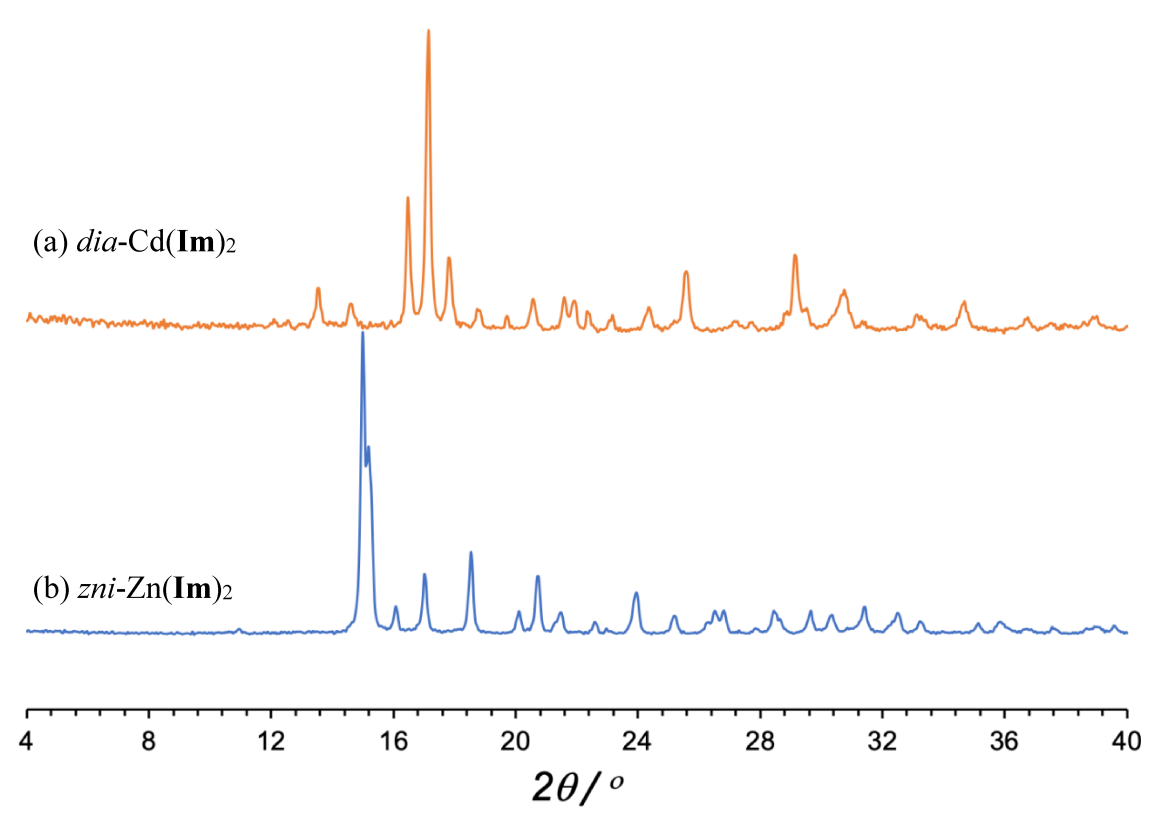


Figure S4. Experimental powder patterns for (a) dia-Cd(Im)₂ and (b) zni-Zn(Im)₂ prepared from solution.

S.4.2 Rietveld refinement of sql-Hg(Im)2 structure

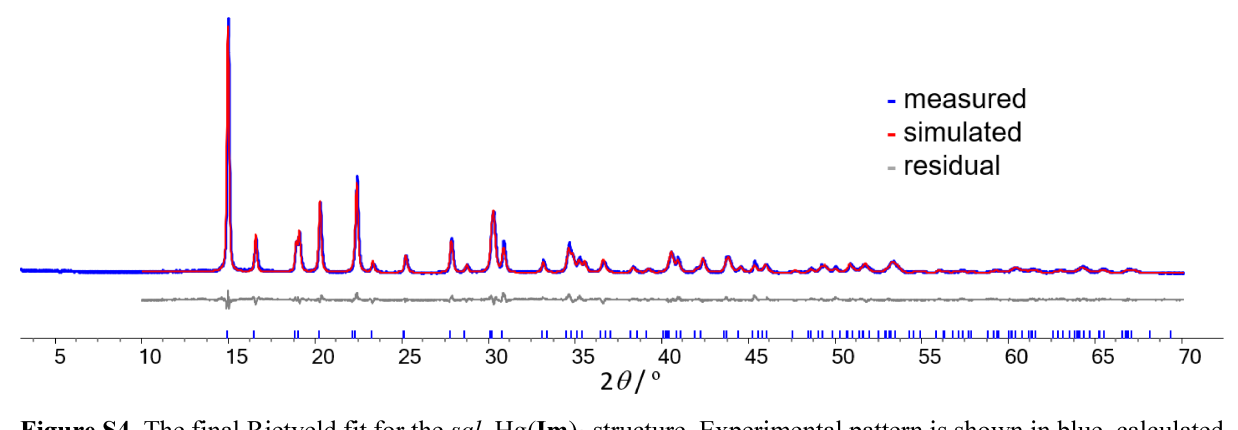


Figure S4. The final Rietveld fit for the sql–Hg(\mathbf{Im})₂ structure. Experimental pattern is shown in blue, calculated pattern in red, and difference curve in grey.

Table S4. Crystallographic data for structure of sql-Hg(Im)₂ polymorph determined from powder X-ray diffraction data.

	sql–Hg(Im) ₂
Formula	Hg(C ₃ H ₃ N ₂) ₂
$M_{ m r}$	334.73
Crystal system	orthorhombic
CSD deposition code	1948341
a / Å	9.4089(4)
b / Å	7.6414(3)
c / Å	5.3625(2)
α (°)	90
β (°)	90
γ (°)	90
V / Å ³	385.549(3)
Space group	$P2_{1}2_{1}2$
$\rho_{\rm c}$ (g cm ⁻³)	2.8835
Radiation type	Cu- $K\alpha$ ($\lambda = 1.5418 \text{ Å}$)
F(000)	300
R _{wp} (%)	9.2
R _p (%)	7.1
R_{Bragg} (%)	2.7
χ^2	1.63

S.5 Thermogravimetric analysis (TGA) of prepared materials

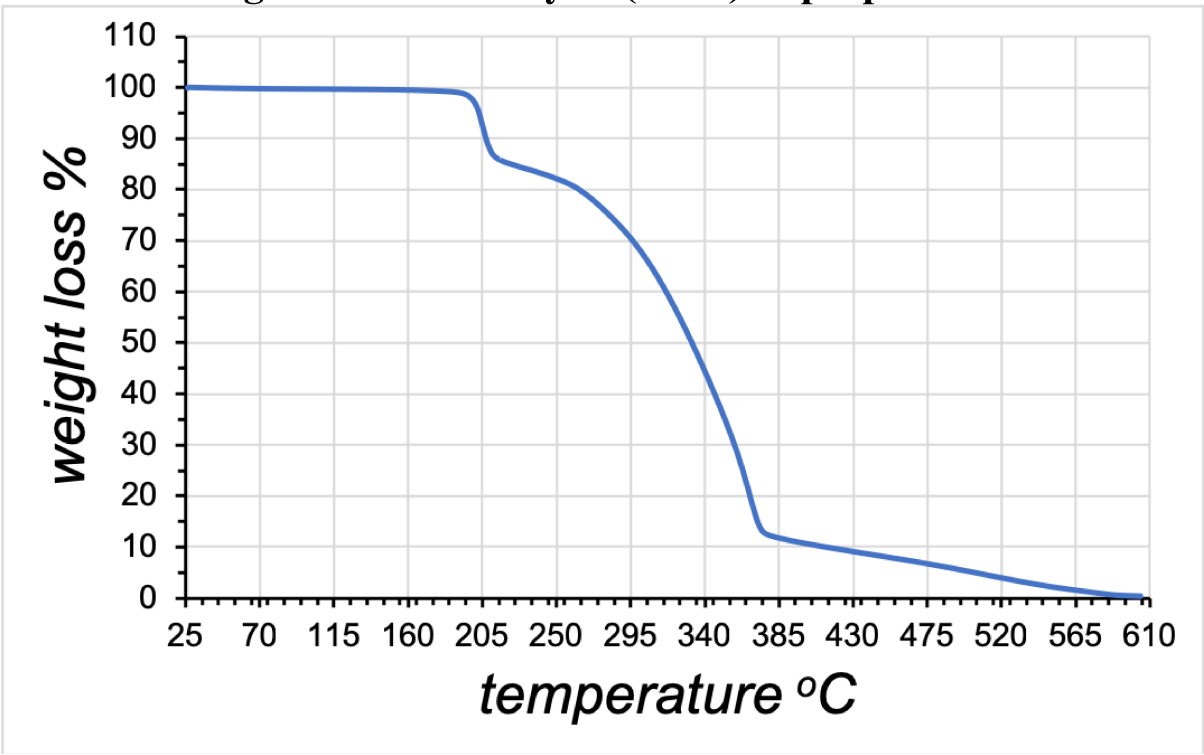


Figure S6. TGA thermogram of *sql*–Hg(**Im**)₂ framework prepared by LAG with MeOH.

S.6 Fourier-transform infrared attenuated total reflectance (FTIR-ATR) spectra

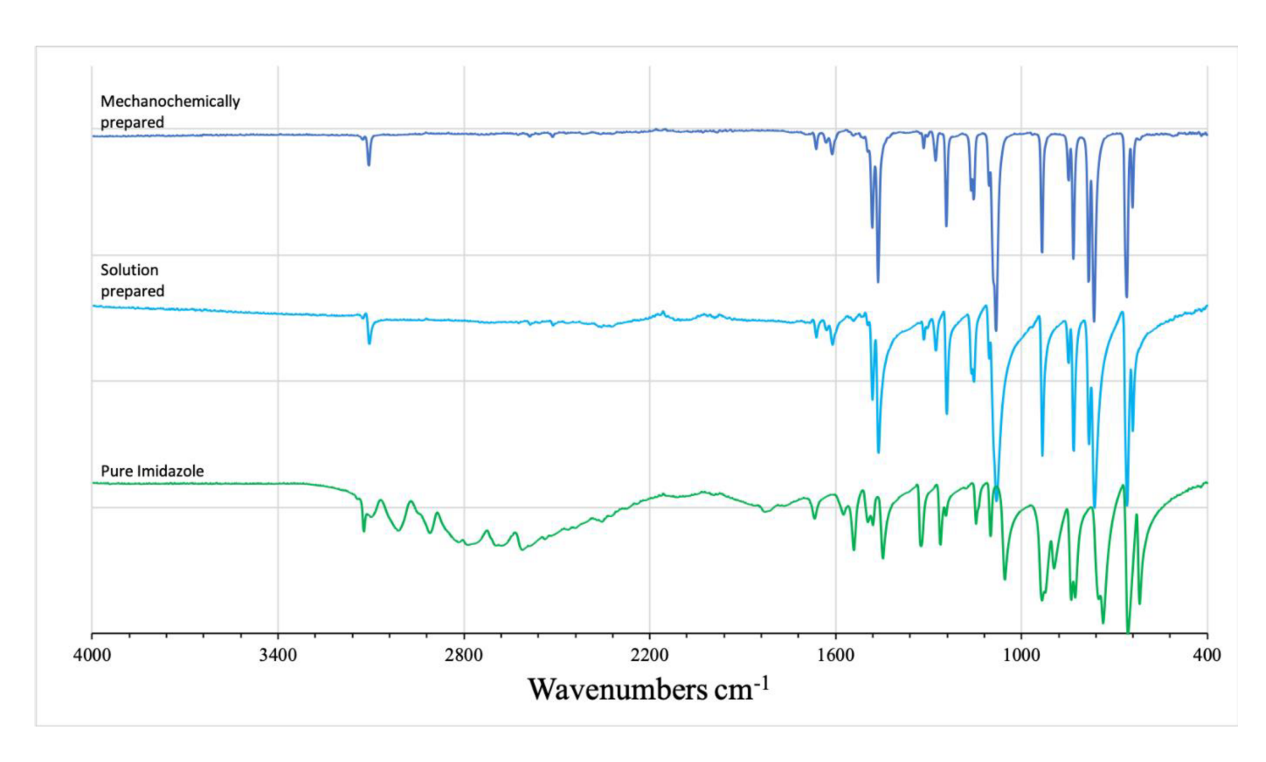


Figure S7. FTIR-ATR spectra of sql-Hg(\mathbf{Im})₂ products and relevant starting materials (from top to bottom): Mechanochemically prepared sample, with MeOH used as the LAG additive; solution-prepared sql-Hg(\mathbf{Im})₂; solid H \mathbf{Im} ligand.

S.7 Solid-state NMR spectroscopy

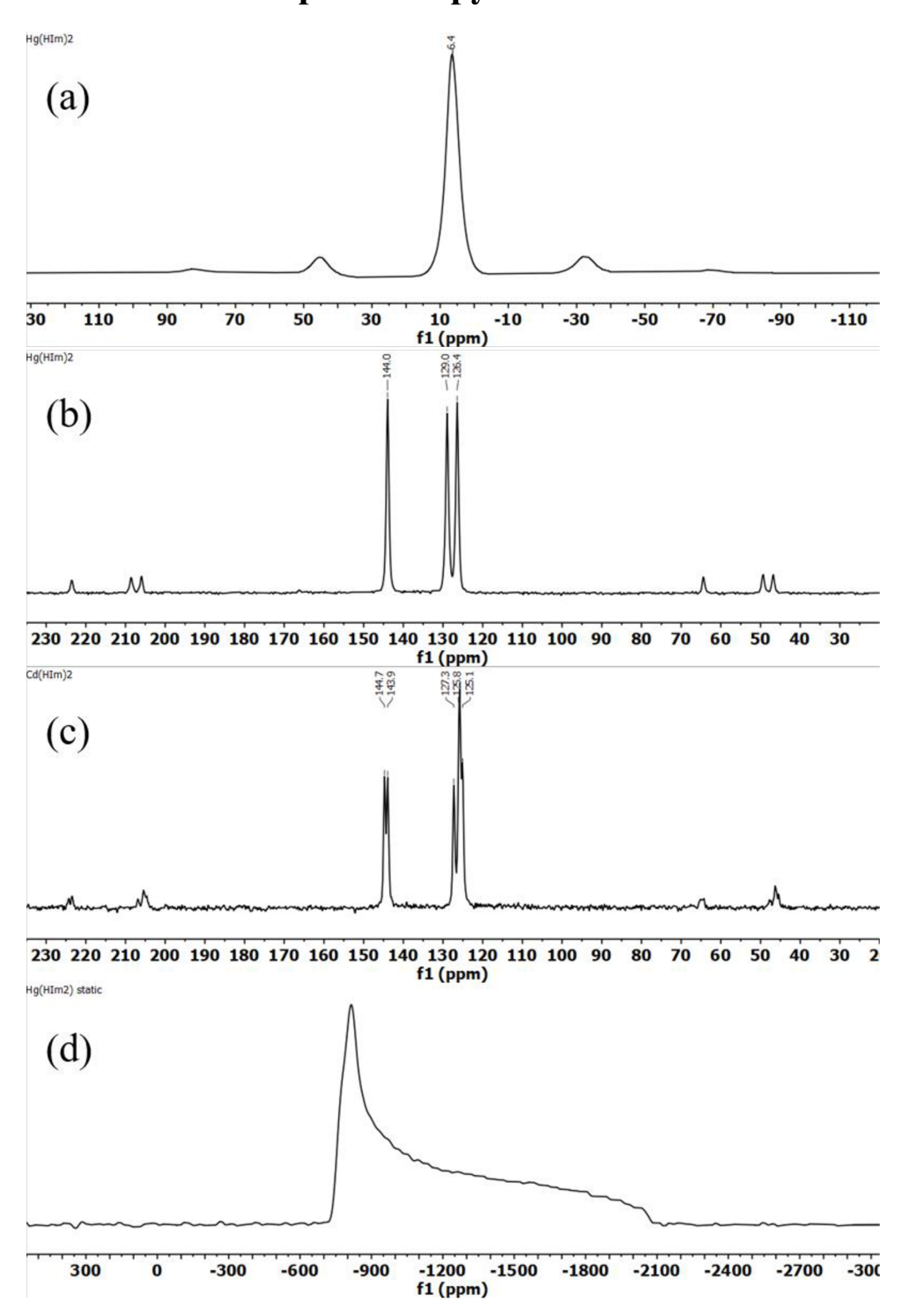


Figure S21. Solid-state NMR spectra of *sql*-Hg(**Im**)₂: a) ¹H, b) ¹³C, c) ¹⁵N, and d) ¹⁹⁹Hg (static). In (a), (b), and (c), only the center bands are labeled with chemical shift values; the other signals are spinning sidebands.

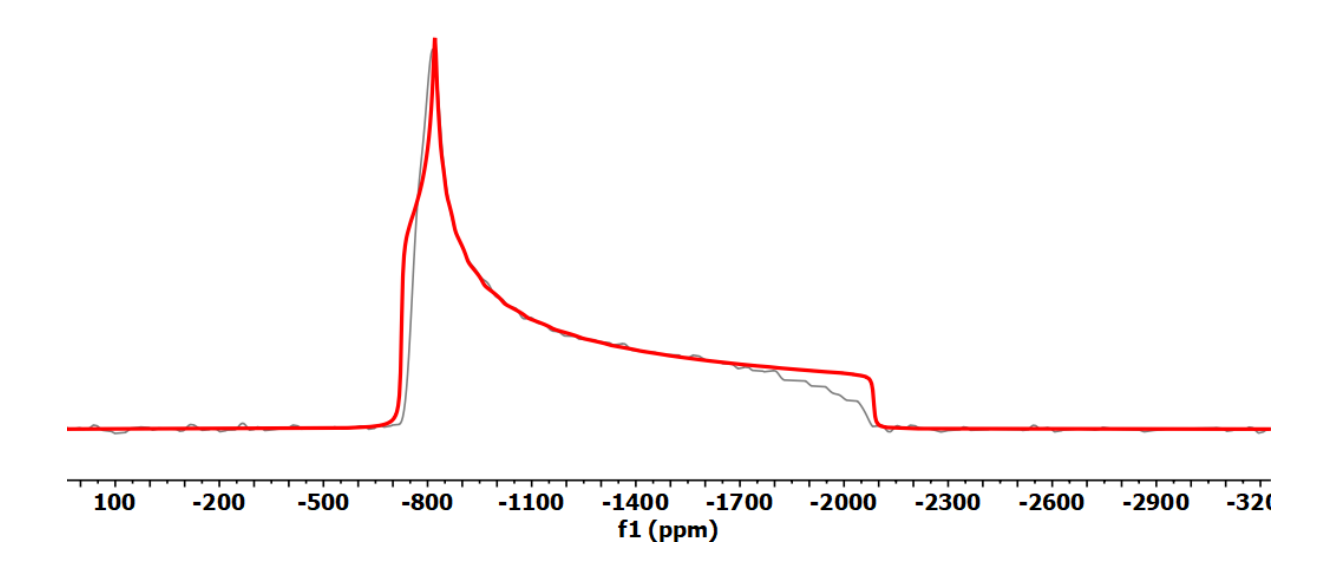


Figure S22. Fit (red) to the static solid-state ¹⁹⁹Hg NMR powder pattern of *sql*-Hg(**Im**)₂ (grey). The pattern shows that the chemical shift tensor at the mercury nucleus has nearly axial symmetry (isotropic chemical shift δ_{iso} = -1212.5 ppm, span Ω = 1366 ppm, skew κ = 0.9).

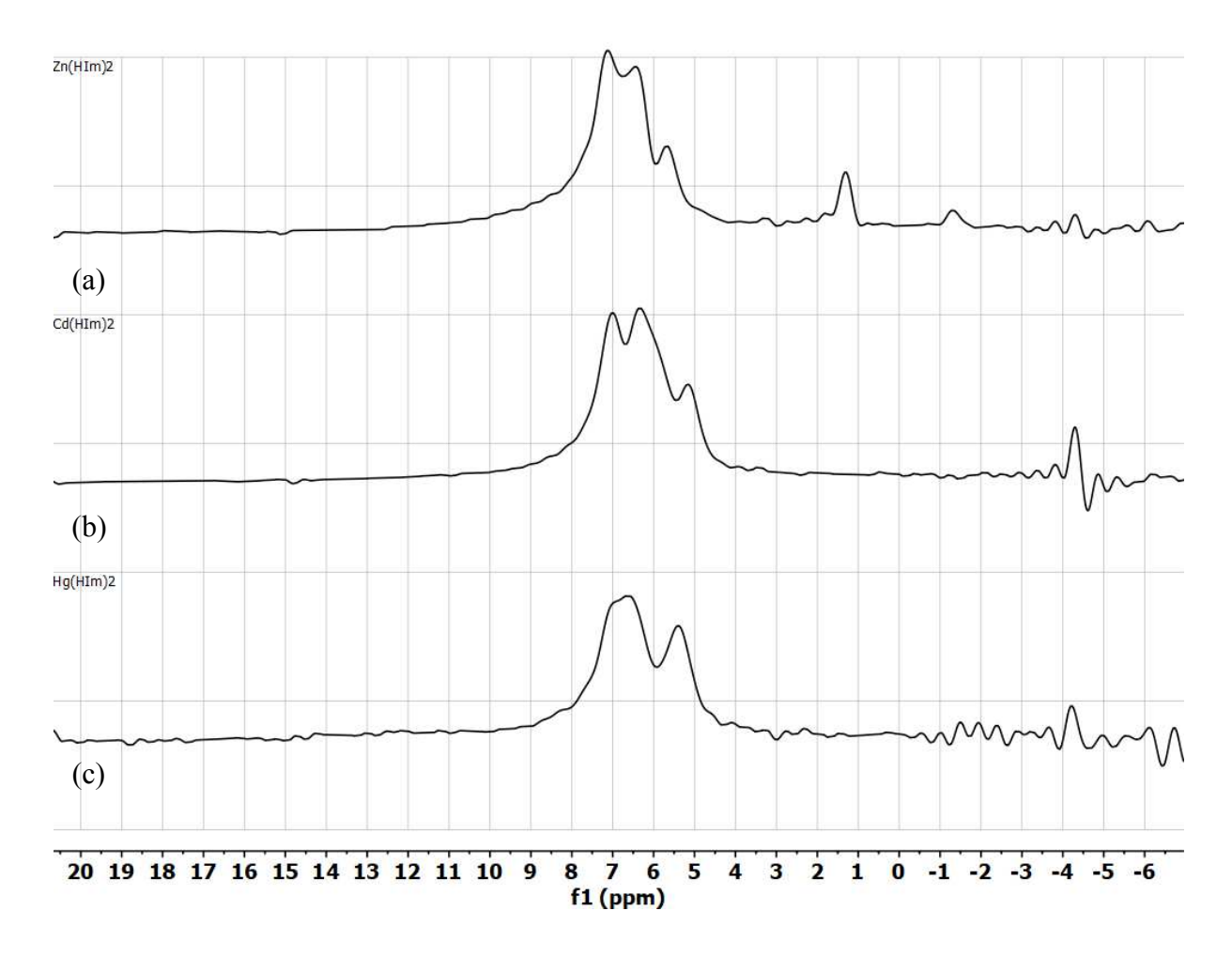


Figure S23. ¹H PMLG-5 ssNMR spectra of (a) *zni*-Zn(**Im**)₂, (b) *dia*-Cd(**Im**)₂, and (c) *sql*-Hg(**Im**)₂. The signals between 5 and 8 ppm are real signals; those at lower ppm values are artifacts of the windowed PMLG sequence.

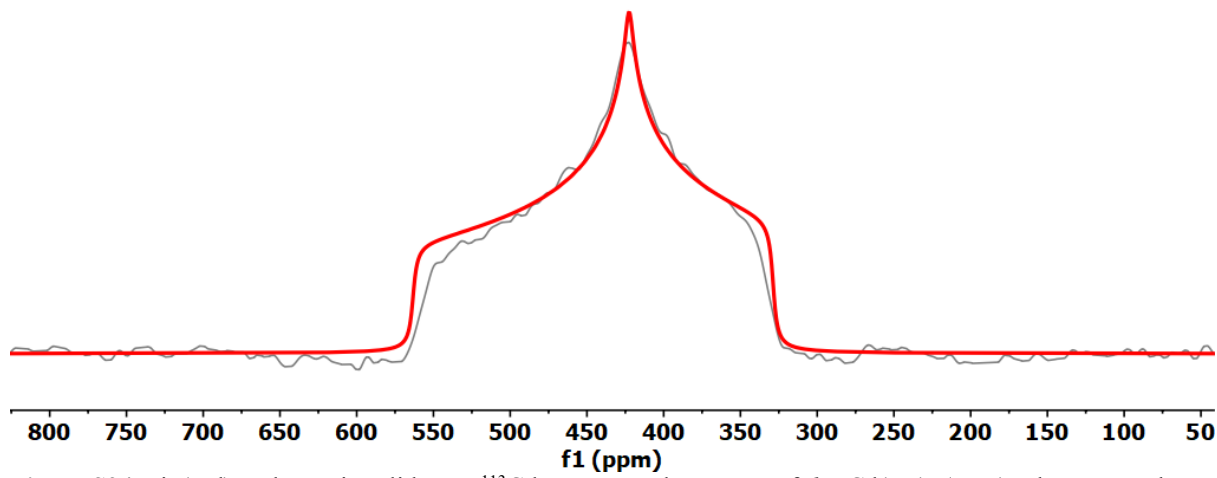


Figure S24. Fit (red) to the static solid-state ¹¹³Cd NMR powder pattern of *dia*-Cd(**Im**)₂ (grey). The pattern shows non-axial chemical shift anisotropy (isotropic chemical shift δ_{iso} = 438.2 ppm, span Ω = 235.0 ppm, skew κ = -0.2).

S.8 Bader Analysis

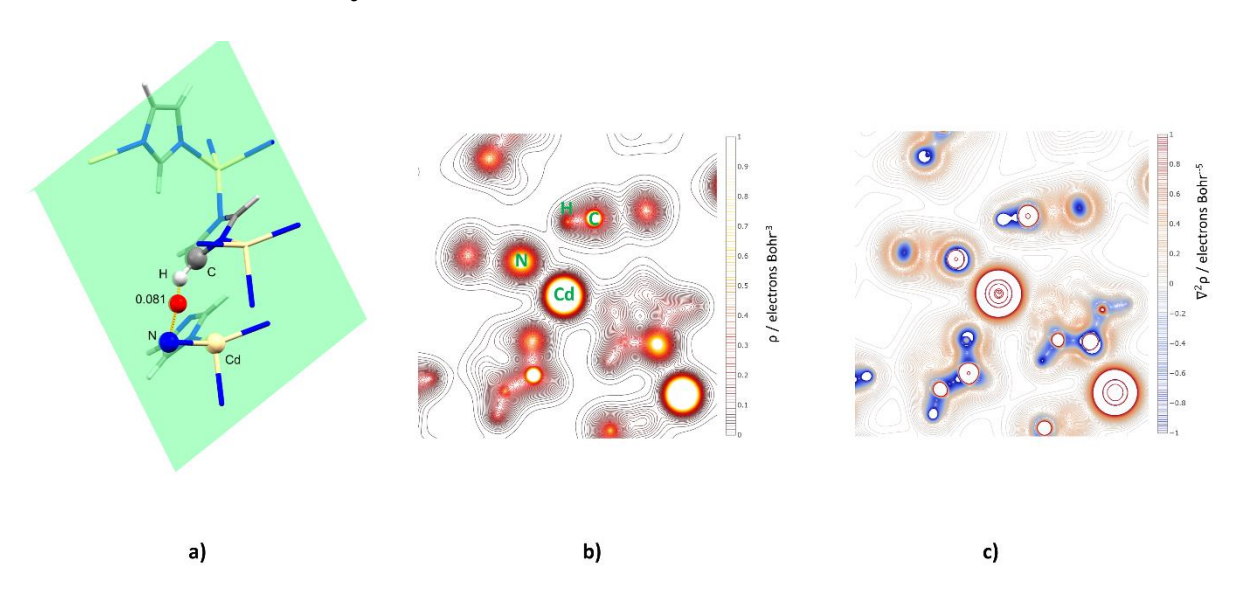


Figure S25. Selected bond critical points of for the hypothetical sql-Cd(**Im**)₂ structure. a) Structure plot showing a C-H···N bonding interaction with a BCP with $\rho = 0.081$ electrons Å-3. The green plane shows the orientation of the contour plot slices. b) 2D contour plot showing the electron density distribution. c) 2D contour plot showing the Laplacian electron density. Both contour plots indicate a weak C-H···N interaction connecting the 2D layers of the sql framework.

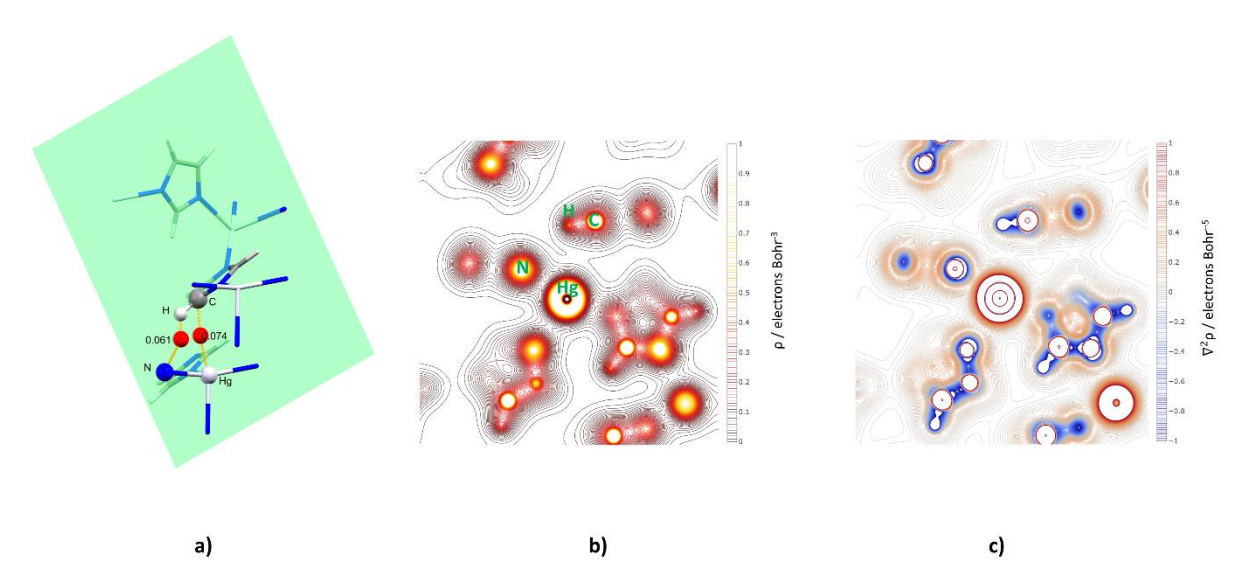


Figure S26. Selected bond critical points of for the sql-Hg(\mathbf{Im})₂ structure. a) Structure plot showing a C-H···N bonding interaction with a BCP with $\rho = 0.061$ electrons Å-³ as well as a C-H···Hg bonding interaction with a BCP with $\rho = 0.074$ electrons Å-³. The green plane shows the orientation of the contour plot slices. b) 2D contour plot showing the electron density distribution. c) 2-D contour plot showing the Laplacian electron density. Both contour plots indicate that the dominant interaction between the 2D layers of the sql framework occurs via Hg atom, unlike the hypothetical sql-Cd(\mathbf{Im})₂ structure where Cd atom does not participate in non-covalent interactions.

S.9 Comparison to other 2-D ZIF structures

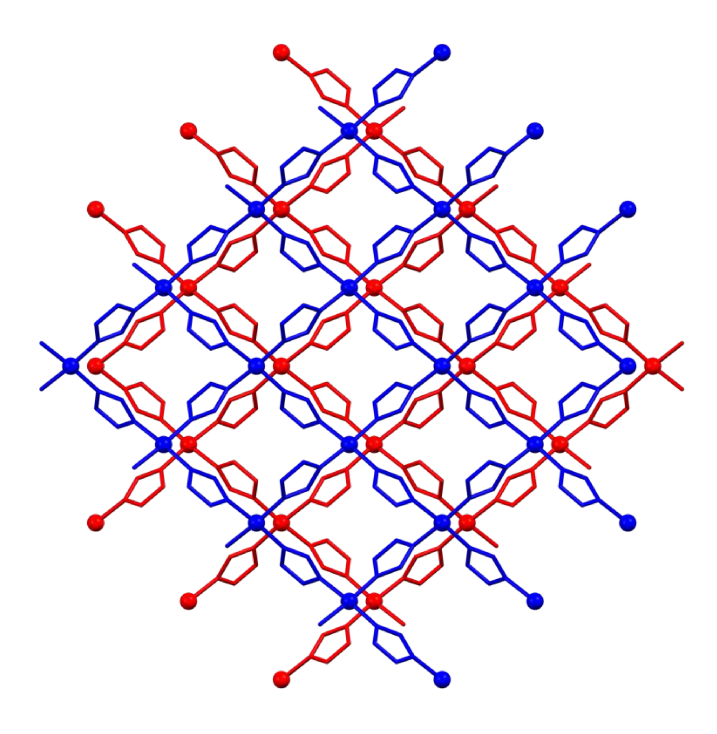


Figure S27. A view of two layers (top layer blue, bottom layer red) of the sql-Ni(Im)₂ framework, perpendicular to the layers and parallel to the crystallographic c-axis (CSD code ALIDUU). Metal atoms are shown as spheres.

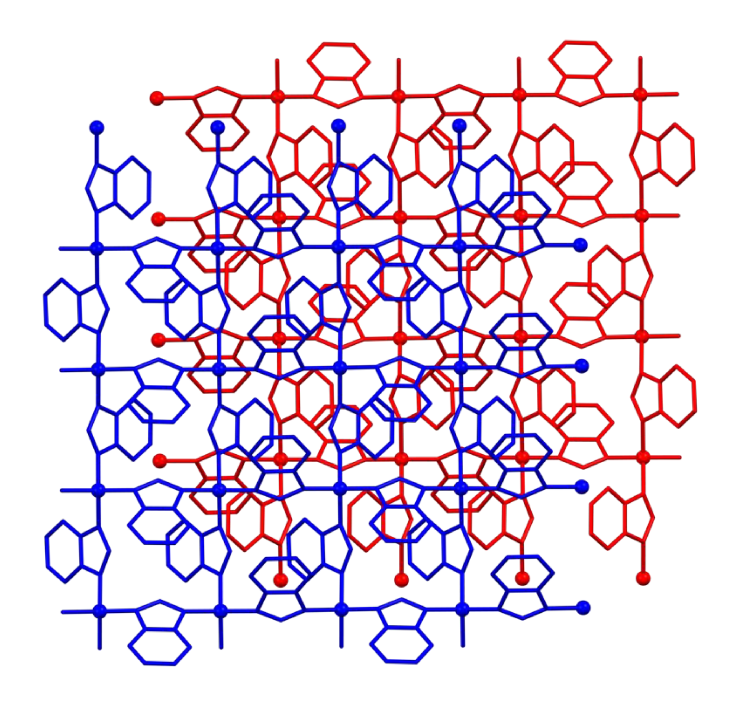


Figure S28. A view of two layers (top layer blue, bottom layer red) of the sql-Zn(Bz**Im**)₂ framework, perpendicular to the layers and the crystallographic ab-plane (CSD code KOLYAM). Metal atoms are shown as spheres.

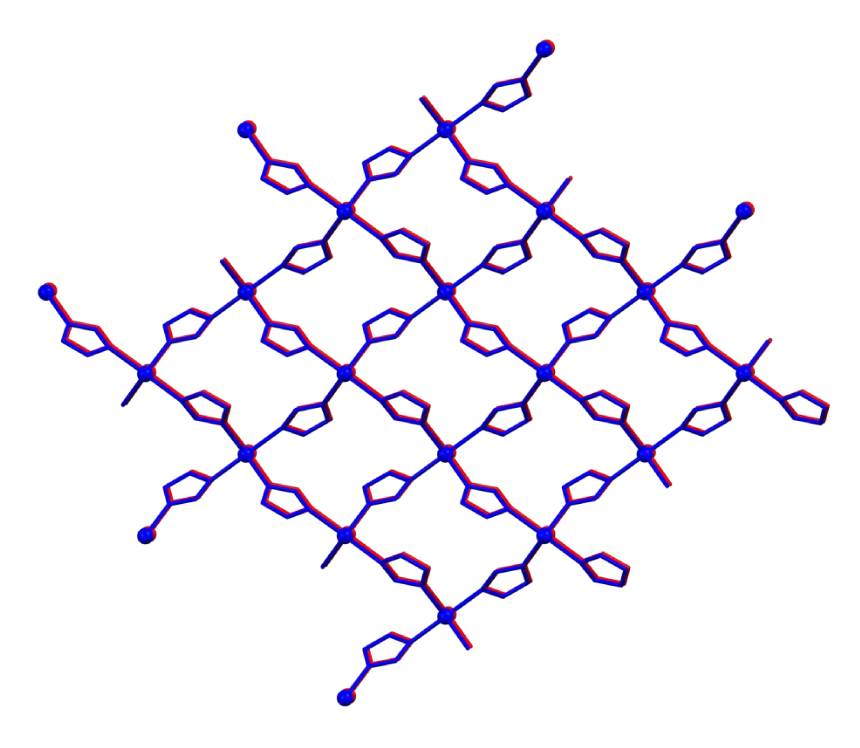


Figure S29. A view of two layers (top layer blue, bottom layer red) of the sql-Hg(\mathbf{Im})₂ framework, approximately normal to the planes and slightly offset from the crystallographic c-axis to illustrate direct stacking of the layers plane. Metal atoms are shown as spheres.

S.10 References

- 1. W. I. F. David, K Shankland, J. van de Streek, E. Pidcock, W. D. S. Motherwell and J. C. Cole. *J. Appl. Crystallogr.* 2006, **39**, 910.
- 2. A. Boultif and D. Louer, J. Appl. Crystallogr. 2004, 37, 724.
- 3. G. S. Pawley, Unit-cell refinement from powder diffraction scans. *J. Appl. Crystallogr.* 1981, **14**. 357.
- 4. A. Coelho, Coelho Software: Brisbane, Australia 2017.
- 5. H. M. Rietveld, Line profiles of neutron powder-diffraction peaks for structure refinement. *Acta Crystallogr.* 1967, **22**, 151.
- 6. R. E. Taylor, Conc. Magn. Reson. A. 2004, 22A, 79.
- 7. P. Betrani, J. Reva and B. Bechinger, Solid State Nucl. Magn. Reson. 2014, 61-62, 15.
- 8. K. J. Harris, A. Lupulescu, B. E. G. Lucier, L. Frydman and R. W. Schurko, *J. Magn. Reson.* 2012, **224**, 38.
- 9. I. Hung, A. J. Rossini and R.W. Schurko, J. Phys. Chem. A. 2004, 108, 7112.
- 10. S. Kidambi and A. Ramamoorthy, *J. Phys. Chem. A* 2002, **106**, 10363.
- 11. S. Hayashi and K. Hayamizu, Bull. Chem. Soc. Jpn. 1991, **64**, 685.
- 12. E. Vinogradov, P. K. Madhu and S. Vega, Chem. Phys. Lett. 1999, 314, 443.
- 13. E. Salager, R. S. Stein, S. Steuernagel, A. Lesage, B. Elena and L. Emsley, *Chem. Phys. Lett.* 2009, **469**, 336.
- 14. I. Huskić, J. C. Christopherson, K. Užarević and T. Friščić, *Chem. Commun.*, 2016, **52**, 5120
- 15. R. Dovesi, A. Erba, R. Orlando, C. M. Zicovich-Wilson, B. Civalleri, L. Maschio, M. Rérat, S. Casassa, J. Baima, S. Salustro and B. Kirtman, *Wiley Interdiscip. Rev. Comput. Mol. Sci.*, **2018**, 8, e1360.
- 16. A. D. Becke, J. Chem. Phys., 1993, 98, 5648.

- 17. C. Lee, W. Yang and R. G. Parr, *Phys. Rev. B*, 1988, **37**, 785.
- 18. S. Grimme, J. Antony, S. Ehrlich and H. Krieg, J. Chem. Phys., 2010, 132, 154104.
- 19. M. F. Peintinger, D. Vilela Oliveira and T. Bredow, J. Comput. Chem., 2013, 34, 451.
- 20. J. Laun, D. Vilela Oliveira and T. Bredow, J. Comput. Chem., 2018, 39, 1285.
- 21. R. Weihrich and I. Anusca, Z. Anorg. Allg. Chem., 2006, 632, 335.
- 22. P. J. Hay and W. R. Wadt, J. Chem. Phys., 1985, 82, 299.
- 23. Y. Dou, R. G. Egdell, D. S. L. Law, N. M. Harrison and B. G. Searle, *J. Phys.: Condens. Matter*, 1998, **10**, 8447.